PAPER

Perspectives for a new realization of the pascal by optical methods

To cite this article: Karl Jousten *et al* 2017 *Metrologia* **54** S146

IOP Publishing | Bureau International des Poids et Mesures Metrologia

Metrologia **54** (2017) S146–S161 https://doi.org/10.1088/1681-7575/aa8a4d

Perspectives for a new realization of the pascal by optical methods

Karl Jousten[1], Jay Hendricks[3], Daniel Barker[3], Kevin Douglas[3], Steve Eckel[3], Patrick Egan[3], James Fedchak[3], Jens Flügge[2], Christof Gaiser[1], Douglas Olson[3], Jacob Ricker[3], Tom Rubin[1], Wladimir Sabuga[2], Julia Scherschligt[3], Rene Schödel[2], Uwe Sterr[2], Jack Stone[3] and Gregory Strouse[3]

[1] Physikalisch-Technische Bundesanstalt (PTB), Abbestr. 2-12, 10587 Berlin, Germany
[2] Physikalisch-Technische Bundesanstalt (PTB), Bundesallee 100, 38116 Braunschweig, Germany
[3] NIST, 100 Bureau Drive, Gaithersburg, MD 20899, United States of America

E-mail: karl.jousten@ptb.de

Received 3 July 2017, revised 23 August 2017
Accepted for publication 5 September 2017
Published 6 November 2017

Abstract

Since the beginning of measurement of pressure in the 17th century, the unit of pressure has been defined by the relationship of force per unit area. The present state of optical technology now offers the possibility of using a thermodynamic definition—specifically the ideal gas law—for the realization of the pressure unit, in the vacuum regime and slightly above, with an accuracy comparable to or better than the traditional methods of force per area. The changes planned for the SI in 2018 support the application of this thermodynamic definition that is based on the ideal gas law with the necessary corrections for real-gas effects. The paper reviews the theoretical and experimental foundations of those optical methods that are considered to be most promising to realize the unit of pressure at the highest level of metrology.

Keywords: SI, pressure realization, vacuum metrology, refractive index, interferometry, optical cavity, absorption

(Some figures may appear in colour only in the online journal)

1. Introduction

In the context of the changes planned for the SI in 2018 [1] the kilogram will be redefined and several physical constants, among them the Boltzmann constant k_B, will be fixed to a certain value. The kelvin will be newly defined by the amount of energy $k_B T$ [2, 3]. This makes the ideal gas law not a new, but a more attractive alternative route with new perspectives for National Metrological Institutes to realize the pressure scale by measuring gas density. Over the past two decades there have been several research activities at The National Institute of Standards and Technology (NIST), Physikalisch-Technische Bundesanstalt (PTB) and the Technical Research Institute of Sweden AB (SP) (now a part of the Research Institutes of Sweden AB, RISE) to measure gas density by optical methods [4–10]. The goal of this paper is to propose the framework for how these optical techniques will provide SI traceability for the pascal with some emphasis on the research programs of NIST and PTB.

The meter convention does not define physical quantities, but is concerned that these are expressed in the International System of Units, the SI [11]. This means that any fundamental physical equation expressing the quantity under consideration can be used to express the unit of the quantity in the SI. It also means that a derived unit can often be expressed in different ways by combining base units with derived units having special names. e.g. the pascal can be written as kg m^{-1} s^{-2}, but also as N m^{-2} (see equation (1) following), because the newton (N), a unit of force, is nothing more than a special name for kg m s^{-2}. Similarly, the Pa may be written as J m^{-3}, (see equation (4) following), because the joule is another name for N m. Since the unit of the pascal can be expressed as J m^{-3}, it is a unit that may be thought of as 'energy per unit volume', or even more simply as 'energy density'.

Traditionally, pressure p is defined as the quotient of the physical quantities of force F and area A, i.e.

$$p = \frac{F}{A}. \tag{1}$$

Herein, a certain force F acts normally on a well defined plane area A. For many practical applications this is a convenient definition, since by knowing p the force F acting on a certain area A can be easily calculated. While equation (1) is a convenient definition for applications where force is the primary concern (for example in structural engineering applications), it is not the best definition of pressure in other applications, such as when we are considering the number of gas molecules in a vacuum chamber. In this regime, the number density of gas molecules is a better definition [12].

For gas pressures, at present there are several types of primary standards in use: mercury-based U-tube manometers and piston gauges give the most accurate realization of pressure around 100 kPa, but may be extended to lower pressures of about 1 Pa with oil-based U-tube manometers, or to higher pressures up to about 1000 MPa using piston gauges. Static and continuous expansion systems extend the scale down to 10^{-9} Pa. These systems, however, need traceability to U-tube manometers or piston gauges to be SI traceable to pressure.

If the primary standard is realized by a piston gauge, the pressure p of a fluid is balanced by the gravitational force of the mass m of a piston plus optional additional mass pieces acting on the effective area A_{eff} of the piston-cylinder assembly

$$p = \frac{mg}{A_{\mathrm{eff}}}. \tag{2}$$

The traceability is accomplished by calibrated mass pieces, the locally known acceleration of gravity g and the geometrically determined effective area.

If the primary standard is realized by a closed U-tube manometer filled with a liquid, a differential pressure p between the evacuated side of the U-tube (at pressure p_0) and the test side of the U-tube is determined by the difference Δh of the height of the liquid in the two tubes with respect to a horizontal plane:

$$p = \rho g \Delta h \tag{3}$$

ρ is the mass density of the manometer fluid.

In both types, it is necessary to have a reference side that is evacuated to a level such that its pressure p_0 is much smaller than p and, in the ideal case, is negligible compared to p.

We endeavour to establish a new kind of primary standard for gas pressure that is based upon Boltzmann's constant, unlike manometers and piston gauges described above which are based on equation (1). Our proposed primary standard for gas pressure applies the ideal gas law in the form

$$p = \rho_{\mathrm{N}} k_{\mathrm{B}} T \tag{4}$$

where ρ_{N} is the number density, i.e. number of molecules N per volume V:

$$\rho_{\mathrm{N}} = \frac{N}{V}. \tag{5}$$

In the SI, the number N can also be expressed in terms of ν, the amount of substance (unit: mole) of the gas species. The proportionality constant that relates them is the Avogadro constant, N_{A}:

$$N = \nu N_{\mathrm{A}}. \tag{6}$$

The relation of k to the molar gas constant R is obtained from another form of the ideal gas law

$$p = \rho_{\nu} R T \tag{7}$$

where ρ_{ν} is the molar density, i.e. the amount of substance ν per volume V. It is evident from equations (4) to (7) that

$$R = k_{\mathrm{B}} N_{\mathrm{A}}. \tag{8}$$

Both N_{A} and k_{B} will be defining constants in the new SI having exact values with no attributed uncertainty. So, also the molar gas constant R will be exact.

As already mentioned, in the new SI, the kelvin will be equal to the change of thermodynamic temperature that results in a change of thermal energy $k_{\mathrm{B}}T$ [3]. Looking at equation (4) it becomes clear that the definition and realization of pressure p by this equation is an appealing way to provide traceability for this derived quantity. This is achieved if the number density ρ_{N} can be accurately measured in a traceable manner. As mentioned earlier, this method is an attractive way to realize pressures in the vacuum range.

Optical methods can provide an accurate measurement of ρ_{N}, because molecules interact with electromagnetic radiation. Whether dispersion, absorption, fluorescence or other light–matter interaction is best exploited depends on the range of pressure, the gas species and desired accuracy of the realization. As is often the case in metrology, the best accuracy can be achieved by using systems that are as simple as possible. e.g. such a system may consist of atoms or molecules in a vacuum (where the ideal gas law applies), well isolated from each other and where their interaction with electromagnetic radiation is calculable *ab initio*. This is essentially the simplest form of the model that we propose for the measurement of ρ_{N} and thus the future for realization of the pascal. Alternately, if pressure can be established by some other means and is treated as a known in equation (4), we can use the density measurement as a future realization of the kelvin in accordance with the *Mise en Pratique* of the kelvin [13].

In section 2 we will outline how well the assumption of isolated molecules is met and what the limits are. In section 3 we shall describe how gas density can be measured by optical methods. We will focus on the measurement models and their assumptions and the possible influence of the assumptions on accuracy and quality of traceability. We include the rate of loss method where molecules are cooled to near 0 K by optical methods, trapped in a magnetic field, lost from the trap by collisions with the surrounding gas molecules and sensed by fluorescence. In section 4 we will review the *ab initio* calculation of the interaction of atoms and molecules with electromagnetic radiation in the meaningful frequency range for refractivity and absorption measurements. Section 5 will outline present or proposed experimental set-ups to realize the optical measurement methods used to determine the number density ρ_{N}. A

discussion of the proposed methods, including the advantages and drawbacks compared to the existing methods of pressure realization will follow in section 6, before we draw some conclusions in the final section.

2. Ideal and real gas

Equations (4) and (7) describe the state of an ideal gas, where the molecules do not interact through long-ranged forces and can be simulated as 'hard spheres' that experience pure elastic collision without any loss of energy. In addition, it is assumed that the volume of all the 'hard spheres' is negligible compared to the macroscopic volume V of the container filled by the gas. In reality, the molecules interact by electromagnetic forces, mainly of the van-der-Waals type, and exhibit a finite internal volume.

Both effects depend on ρ_N, or equivalently ρ_ν:

- The internal volume of all molecules, which is related to the total volume V, is proportional to N or ρ_N
- In general, when the molecules are far apart from each other, there will be no force between them. When two molecules approach each other, the electron clouds first attract, then overlap brings strong repulsive forces into play. The total collision rate is proportional to ρ_N^2 or ρ_ν^2 and will cause a deviation from the ideal gas law.

When the above considerations are taken into account, a description for a 'real gas' is given by the following power series in ρ_ν:

$$p = \rho_\nu RT\left(1 + B(T)\,\rho_\nu + C(T)\,\rho_\nu^2 + \ldots\right), \qquad (9)$$

where $B(T)$ is the density virial coefficient of second order, $C(T)$ of third order. These and the higher coefficients depend on temperature T. Higher orders take into account multi-molecule collisions, the change of collision rate with effective molecule diameter etc. It is clear that the influence of higher orders drops rapidly with lower pressures, particularly at gas pressures less than one atmosphere (referred to as the vacuum regime).

The temperature dependence of the virial coefficients can be understood by the interplay of kinetic and potential energy: When the temperature and kinetic energy of the molecules is low, the weakly attractive force between molecules has a significant influence and causes the pressure to be reduced compared to an ideal gas. When the kinetic energy of the molecules is high, the weak attractive force is less important than the strong repulsive force and the pressure reduction is less strong or even positive (B increases) for some gas species. At very high temperatures the kinetic energy allows the molecules to run against the repulsive force allowing them to move closer together which causes the pressure (and B) to slightly decrease again.

For estimating the influence of different virial coefficients on the realisation of the pascal, table 1 gives values of the pressure correction caused by the specific coefficients. The dominating term due to real gas properties arises from the second density virial coefficient $B(T)$. For helium, starting with the first *ab initio* calculation [14], this virial coefficient has been extensively studied during the last 15 years by several groups of theorists. The most recently published calculated values are given in [15]. The values are in very good agreement with *ab inito* values derived in [16] and with the experimental value obtained in [17] at $T = 273.16\,\mathrm{K}$.

Table 1. Relative pressure correction $\delta p/p$ caused by the virial coefficients B and C, as well as the second refractivity virial coefficient b_R (see section 4) calculated at 273 K using the literature data for B, b_R and C (for references see section 2 (He) and section 6 (Ar)).

	$\delta p_B/p$ (parts in 10^6)		$\delta p_{b_R}/p$ (parts in 10^6)		$\delta p_C/p$ (parts in 10^6)	
p (Pa)	He	Ar	He	Ar	He	Ar
1	0.005	0.007	0.000	0.000	0.000	0.000
10	0.05	0.07	0.000	0.002	0.000	0.000
100	0.5	0.7	0.004	0.017	0.000	0.000
1000	5	7	0.044	0.17	0.000	0.000
10 000	50	70	0.44	1.7	0.002	0.018
100 000	500	700	4.4	17	0.2	1.8

For the third virial coefficient, theoretical calculations are much more involved and therefore only one *ab initio* calculation is available [18] together with the result of a simplified theory by [15]. Experimental values have been published by several groups, the last one in [17], and the agreement is more than sufficient regarding the small influence at low pressures (see table 1).

3. Measurement of number density of gas by optical methods

3.1. Refractive index method

Electromagnetic (EM) waves travelling through a gaseous medium interact with the electrons and to a lesser extent with the nuclei of the molecules in that medium. Depending on the frequency of the EM wave, either absorption or dispersion occurs. In the case of absorption, the frequency of the EM wave is in resonance with one of the possible molecule quantum state transitions. In the case of dispersion, even if the frequency is far from resonance, the EM wave polarizes the molecules with the net effect of reducing the speed c of the EM wave and the wavelength λ. The reduction depends on the frequency ν of the EM wave and is described by the refractive index $n(\nu)$:

$$c = \frac{c_0}{n(\nu)} \qquad (10)$$

with c_0 the speed of light in an ideal vacuum.

From this equation, it is shown that the simplest description of refractive index of a gas is the ratio of the speed of light in vacuum divided by the speed of light in the gas at a given pressure. The relation of n to ρ_N for an isotropic homogeneous medium is obtained by the Lorentz–Lorenz equation [19]. An EM wave with frequency ν induces in each molecule an oscillating dipole with frequency ν. All the emitted dipole waves give rise to an effective field acting on other dipoles. Therefore, two electric fields, the incident field $\mathbf{E}$ of the EM

wave and the sum $\sum \mathbf{E}_{jl}$ of all oscillating dipole fields $\mathbf{E}_{jl}$ (the field from dipole l at the position of dipole j), make up the total field acting on dipole j. The sum extends over all dipoles except the jth one. If we assume a non-magnetic medium, the magnetic field will not influence the dynamic equilibrium.

The secondary electric field created by the oscillating dipoles has a very interesting consequence, known as the extinction theorem [19]: The incident wave may be regarded as extinguished at any point within the medium by destructive interference with the dipole field and replaced by a wave of propagation with a different velocity described by equation (10). This extinction theorem can be proved by integral equations, but also in the framework of Maxwell's electromagnetic theory. As a consequence of the extinction theorem the relation, known as Lorentz–Lorenz equation, holds:

$$\frac{\alpha}{3\,\varepsilon_0}\rho_\mathrm{N} = \frac{N_\mathrm{A}\alpha}{3\,\varepsilon_0}\rho_\nu = A_\mathrm{R}\rho_\nu = \frac{n^2-1}{n^2+2} \tag{11}$$

where α is the dynamic polarizability of the individual molecule and A_R the molar dynamic polarizability. This equation is entirely analogous to the Clausius–Mossotti equation of electrostatics. It has to be repeated that this equation is true in general, but two basic assumptions need to be made:

(1) The primary limitation of equation (11) is the assumption that interatomic or intermolecular forces between gas atoms or molecules do not affect the interaction with the electromagnetic field. These can be taken into account by introducing refractivity virial coefficients in a manner analogous to equation (9).
(2) In addition, equation (11) does not include magnetic effects, which are small but have a non-negligible influence on measurements of the highest accuracy. Non-zero magnetic susceptibility χ can be taken into account by replacing α with $(\alpha + \chi)$ in equation (11).

The refractive index in the visible spectrum is >1, but for gaseous media it is also very close to 1. For this case equation (11) can be simplified to:

$$\frac{\alpha}{2\varepsilon_0}\rho_\mathrm{N} = n - 1 \tag{12}$$

showing that the refractivity, $n-1$, is approximately proportional to ρ_N. Deviations from the linear approximation are about 0.3% for nitrogen (or air) at 20 °C and 10^5 Pa. This shows that for highest accuracy, the simplification of equation (12) cannot be made.

The interatomic or intermolecular forces can be taken into account by introducing refractivity virial coefficients b_R and c_R in a manner analogous to equation (9):

$$\frac{n^2-1}{n^2+2} = A_\mathrm{R}\rho_\nu\left(1 + b_\mathrm{R}(T)\,\rho_\nu + c_\mathrm{R}(T)\,\rho_\nu^2 + \ldots\right). \tag{13}$$

Note that b_R and c_R must not be confused with the often defined refractivity virial coefficients $B_\mathrm{R} = A_\mathrm{R}b_\mathrm{R}$ and $C_\mathrm{R} = A_\mathrm{R}c_\mathrm{R}$. Equation (13) does not include magnetic effects, which are very small but can be added to the dominating terms [20] as described before for the magnetizability.

To express pressure in terms of the refractive index a combination of equation (9) and equation (12) is needed. In an analogous case to that of the dielectric constant, described in detail in [21], an expression can be easily derived in this paper. Comparable to the measurement of capacitances with and without gas for dielectric-constant gas thermometry, the resonance frequency of a mode-locked (see section 5.1) optical cavity is measured with $\nu(p)$ and without gas $\nu(0)$ for determining the refractive index n. In a simplified case of a non-deformable cavity (effective compressibility equal to zero, $\kappa_\mathrm{eff} = 0$), this would lead to the following quantity deduced from experiment

$$\mu_{\kappa=0} = \frac{\left(\frac{\nu(0)}{\nu(p)}\right)^2_{\kappa=0} - 1}{\left(\frac{\nu(0)}{\nu(p)}\right)^2_{\kappa=0} + 2}. \tag{14}$$

Following the derivation of a working equation in [21], a combination of the equation (9), (13) and (14) leads to the following p versus $\mu_{\kappa=0}$ relation:

$$p = \frac{RT}{A_\mathrm{R}}\left(\mu_{\kappa=0} + \mu^2_{\kappa=0}\frac{(B-b_\mathrm{R})}{A_\mathrm{R}} + \mu^3_{\kappa=0}\frac{C - 2Bb_\mathrm{R} + 2b_\mathrm{R}^2 - c_\mathrm{R}}{A_\mathrm{R}^2} + \ldots\right), \tag{15}$$

Giving up the assumption of no deformation, for a homogenously deformed cavity, the change $l(p)/l(0) = (1 + \kappa_\mathrm{eff}p)$ of the length l with pressure is the relevant deformation, where κ_eff is the effective length compressibility of the cavity, leads to:

$$\frac{\left(\frac{\nu(0)}{\nu(p)}\right)^2 - 1}{\left(\frac{\nu(0)}{\nu(p)}\right)^2 + 2} = \frac{(1+\kappa_\mathrm{eff}p)^2\cdot n^2 - 1}{(1+\kappa_\mathrm{eff}p)^2\cdot n^2 + 2} \approx \frac{(1+2\kappa_\mathrm{eff}p)\cdot n^2 - 1}{(1+2\kappa_\mathrm{eff}p)\cdot n^2 + 2} = \mu. \tag{16}$$

In the approximated term of equation (16), the extremely small $(\kappa_\mathrm{eff}p)^2$ term was discarded. The combination of equations (9), (13) and (16) leads finally to:

$$p = \frac{RT}{A_\mathrm{R} + \frac{2\cdot\kappa_\mathrm{eff}RT}{3}}\left(\mu + \mu^2\frac{\left(B - b_\mathrm{R} - \frac{2\cdot\kappa_\mathrm{eff}RT}{3}\right)}{A_\mathrm{R} + \frac{2\cdot\kappa_\mathrm{eff}RT}{3}} + \ldots\right), \tag{17}$$

where terms cubic in μ have been discarded but should be included when doing precise measurements at high pressures. Beside the fact that the κ_eff term is multiplied by the factor 2, equation (17) is a complete analogy to the expression for dielectric measurements [21]. Equation (17) shows that the significant impact of the compressibility is mainly linear. For an optical cavity made from a typical glass, $\kappa_\mathrm{eff} = 1/(3B) \approx 10^{-11}$ Pa^{-1}, where B is the bulk modulus. Neglecting this compressibility would lead to a measurement error of 3% with helium and 0.37% with argon. This shows that the deformation of the cavity is one of the main challenges of this technique.

Conceptually, all the discussion above applies to the fixed length optical cavity discussed in section 5.1, but the details of the method in section 5.1 are different, requiring some modification of the analysis. Rather than measuring optical frequencies directly, a more attractive approach is based on measurements of the difference frequency between a reference cavity and a measurement cavity. For the device described

in section 5.1, both the reference and measurement cavities are subject to changing pressure, and in principle this would largely cancel the effects of uniform pressure distortions (bulk modulus) that are discussed above. In practice, the effect of bulk modulus continues to play a role for reasons discussed in the references [9, 22].

3.2. Absorption method

In the case of absorption, the frequency ν of the EM wave is in resonance with one of the possible molecule quantum state transitions of the gas molecules in the medium through which the EM wave is travelling and is described by the following:

$$h\nu = E_2 - E_1, \tag{18}$$

where E_1 and E_2 are the corresponding energy levels of the quantum states $|1\rangle$ and $|2\rangle$. Absorption occurs when the molecule's energy state is increased by the absorption of the photon with energy $h\nu$. This normally unstable state of the molecule decays by either spontaneous emission or by stimulated emission from ambient black body radiation or from the present EM wave. The probability for the first event is independent of the surrounding electromagnetic field, the second is proportional to the energy density of the surrounding electromagnetic field as is also the case for absorption.

When the number density of molecules is measured by absorption, it is important that the probability for spontaneous emission P_{spont} is much larger than the one for stimulated emission P_{stim}. The extent to which this condition is fulfilled needs to be checked in each special case and depends on the molecular transition and the incident laser power density. As an example, in thermal equilibrium the ratio due to black body radiation is given by

$$\frac{P_{\text{spont}}}{P_{\text{stim}}} = \exp\left(\frac{h\nu}{kT}\right) - 1. \tag{19}$$

Near 296 K and at a frequency of $3 \cdot 10^{14}$ Hz ($\lambda = 1$ μm) P_{spont} is about 10^{21} times larger than P_{stim}, for $6 \cdot 10^{13}$ Hz ($\lambda = 5$ μm) still by a factor of 10^4 greater, but for wave lengths >5 μm stimulated emission can play a significant role for black body radiation.

When absorption occurs, the amplitude of the EM wave is reduced along the path in the gas. It is the incident power that can be measured by a physical detector. This incident power per area (in radiometry called irradiance, in spectroscopy intensity, I) is proportional to the square of the amplitude of the EM wave. The amount of energy absorbed by the gas, ΔI, is equal to that lost from the initial intensity $I(z)$ (before it passes through a differential path length Δz). Hence, for a wave at frequency ν, the loss of intensity in traversing Δz is given by

$$\Delta I(\nu) = -k(\nu)\, I(\nu, z)\, \Delta z, \tag{20}$$

with $k(\nu)$ the absorption coefficient describing the reduction of intensity.

Normally, absorption and dispersion are described by the complex number $\widehat{n}(\nu)$,

$$\widehat{n}(\nu) = n(\nu) - \mathrm{i}\kappa(\nu), \tag{21}$$

where the imaginary part κ describing absorption is significant only near a molecular transition.

$k(\nu)$ is proportional to the imaginary part of the refractive index $\kappa(\nu)$, equation (21) and its frequency dependence can be described by many sophisticated line shape functions [23–29], the most wide-spread being the Voigt-profile which is a convolution of a Gaussian function and a Lorentz function. The latter describes the frequency dependence of a damped harmonic oscillation, and the Gaussian function describes the Doppler broadening due to the molecular motion.

For accurate measurements of gas density by absorption, $k(\nu)$ must be described by a single line transition and not be influenced by neighbouring absorption lines. In addition, $k(\nu)$ needs to be independent from I. This is the case, when the population density between upper and lower state is not significantly disturbed by the incident EM wave (linear absorption) which needs to be checked in each particular case and depends on the depletion and refilling rate of the two involved states $|1\rangle$ and $|2\rangle$. Note that the depletion and refilling rates are influenced by several factors, including fluorescence into other states, by collisions, by diffusion in and out of the interaction volume of the EM wave, and the (laser) intensity of the EM wave.

When the above considerations are taken into account, the case of linear absorption of equation (20) takes the following form:

$$I(\nu, z) = I_0(\nu) \exp\{-k(\nu)\, z\}, \tag{22}$$

where $I(\nu)$ is the transmitted intensity at ν after passing through a path length z in the medium and $I_0(\nu)$ is the incident intensity entering the absorbing medium.

To relate this to quantities generally used in absorption spectroscopy we change to wave numbers

$$\nu' = \frac{\nu}{c} = \lambda^{-1}, \tag{23}$$

and write

$$k(\nu') = S \cdot \Phi(\nu' - \nu'_{\text{c}}) \cdot \rho_{\text{N}}, \tag{24}$$

where ρ_{N} is the number density of the absorbing molecules, S is the so called line intensity or line strength of the molecular transition, and $\Phi(\nu' - \nu'_{\text{c}})$ is the form or line shape function with the line center at ν'_{c}, for which

$$1 = \int_{-\infty}^{\infty} \Phi(\nu' - \nu'_{\text{c}})\, \mathrm{d}\nu'. \tag{25}$$

Also we denote the total path length through the medium with L and rewrite equation (22) as

$$I(\nu', L) = I_0(\nu') \exp\{-S \cdot \Phi(\nu' - \nu'_{\text{c}}) \cdot \rho_{\text{N}} \cdot L\}. \tag{26}$$

In spectroscopic practice, it is rather difficult to accurately determine ν' and to accurately know Φ at the same position ν'. (Among other influences, the line shape depends on the particular transition and the temperature). For this reason, only the measurement of the complete absorption profile of the line will lead to a high accuracy determination of gas density.

There are basically two approaches to determine ρ_N for a known S [29]: parametric line shape fitting and non-parametric numerical integration over the spectrum. The latter method can be handled analytically in an easier manner and we prefer to present this method of evaluation.

After taking the logarithm of equation (26) and integrating over the full spectrum, we obtain the absorbance curve area A_{line}:

$$A_{\text{line}} = -\int_{-\infty}^{+\infty} \ln\left\{ {}^{I(\nu')}\!/\!_{I_0(\nu')} \right\} \mathrm{d}\nu' = S \cdot \rho_N \cdot L. \tag{27}$$

Hence, the gas number density is determined by the numerical integral A_{line}, the line strength S and the path length L:

$$\rho_N = \frac{A_{\text{line}}}{S \cdot L}. \tag{28}$$

We repeat that this model equation is valid for linear absorption, negligible induced emission and a sufficiently isolated line. Finally we note that only the gas density (or partial pressure) of the interacting molecules can be measured and a pure gas of this kind is needed when the measured gas density (partial pressure) must be identical to the total gas density (total pressure).

3.3. Rate of loss method

Since the early days of laser-cooling and trapping of ultra-cold atoms, it has been known that the loss-rate of ultra-cold atoms from a magnetic trap is largely determined by collisions of the background gas in the vacuum with the ultra-cold atoms [30]. We propose to invert this relationship, thus employing an ensemble of trapped ultra-cold atoms to act as a sensor of the background gas density in the vacuum. To date, a wide variety of atoms have been laser-cooled and trapped, but the alkali-metal atoms are the best candidates for vacuum sensor atoms because of their hydrogen-like atomic structure and the availability of low-cost lasers with wavelengths near the resonant transitions. The ensuing discussion in this section will assume that alkali-metal atoms are the sensor atoms, although much of the discussion can be generalized to other atoms. The collisional loss-rate of ultra-cold atom density ρ_S from a magnetic trap is given by

$$\frac{\mathrm{d}\rho_S}{\mathrm{d}t} = -k_{\text{loss}}\rho_N\rho_S - k_2\rho_S^2 - k_3\rho_S^3. \tag{29}$$

The first term represents the loss of ultra-cold atoms due to collisions with the background gas of density ρ_N in the vacuum and is the quantity of interest; this will be discussed in detail below. The second term is the loss rate due to inelastic two-body collisions between sensor atoms in the trap. For alkali atoms, these collisions are typically mediated via the magnetic dipole–dipole interactions. Such collisions can cause the internal angular momentum to change in one of the atoms. To conserve angular momentum, the atom is excited to a higher angular momentum state of the trap. Typically, the energy stored in the internal angular momentum of the atom is large compared to the trap depth, and thus these collisions result in loss. The third term represents a three-body loss rate among sensor atoms in the trap, i.e. three atoms interact to form an alkali dimer while a third atom absorbs the excess momentum. The kinetic energy of the dimer and third atom are typically much larger than the trap depth, and thus all three are ejected. To disentangle these loss mechanisms and ensure that the loss rate is accurately correlated to the gas density, we consider the timescales of the various loss mechanisms at density scales of interest. Mechanisms with timescales that are significantly different in magnitude or character (i.e. non-exponential) from loss due to background collisions can be separated out. For $\rho_S \sim 10^{10}$ cm^{-3}, the time scale for the k_{loss} term will typically dominate those of k_2 and k_3. Consider, for example, ^{87}Rb as a sensor atom in an extreme high vacuum (XHV) background with $\rho_S \sim 10^{10}$ cm^{-3}. For ^{87}Rb, there are three magnetically trappable states: $|1,-1\rangle$, $|2,2\rangle$, and $|2,1\rangle$ (here we use the notation $|F,m_F\rangle$, where F is the total angular momentum of the atom and m_F is the total angular momentum component along the axis defined by the external magnetic field). Suppose we choose to magnetically trap the $|1,-1\rangle$ state for use as sensor atoms. The time scale for $k_{\text{loss}}\rho_N$ is approximately 2×10^4 s for background hydrogen density of $\rho_N = 10^4$ cm^{-3} (XHV). This timescale is inversely proportional to the background density ρ_N and will thus become smaller as the background density increases. This is much smaller than the time scale for the two-body loss rate, which is $>3 \times 10^6$ s for magnetic fields less than 0.1 mT or that for three-body loss, which is 2×10^8 s at low magnetic fields. In general, the contributions of k_2 and k_3 can be minimized by the proper choice of sensor atom and trapped state. In addition, only the k_{loss} term can be modelled by a single exponential function, which allows the loss-rate due to collisions with the background gas to be distinguished from the other loss rate terms. Therefore, the k_2 and k_3 terms in equation (29) can be neglected. In designing the apparatus, one must also consider non-collisional loss rates, such as those due to spin-flips caused by non-adiabatic transition through a zero in the magnetic field, or by evaporative cooling. The former can be eliminated by proper choice of magnetic field configuration (such as the Ioffe–Pritchard trap [31, 32]), and the latter by proper choice of atom. A detailed examination of the loss-rate mechanisms is the subject of a manuscript under preparation by the authors.

Having disentangled other loss mechanisms as described above, the number density of ultra-cold atoms in a magnetic trap can be modelled as exponentially dependent on the loss-rate:

$$\rho_S = \rho_{S,0}\mathrm{e}^{-t/\tau}. \tag{30}$$

The measured loss-rate is given by

$$\tau^{-1} = k_{\text{loss}}\rho_N, \tag{31}$$

where k_{loss} is a loss-rate coefficient; a fundamental atomic property that may be written as the thermally-averaged collision cross section

$$k_{\text{loss}} = \langle \nu\sigma \rangle \tag{32}$$

where $\sigma = \sigma(v)$ is a total collision cross section between an ultra-cold atom and an ambient molecule in the vacuum with a velocity (v) distribution consistent with thermodynamic

equilibrium (compared to the ambient gas molecules, the low temperature and narrow velocity distortion of the ultra-cold atoms makes the difference between lab-frame and center-of mass velocity irrelevant). The pressure may then be determined via equation (4). Thus using cold-atoms to sense the number density of gas in the vacuum is both an absolute vacuum sensor and primary standard because it depends on a measured loss-rate (time) and fundamental atomic property k_{loss}.

Presently, k_{loss} is known from semi-classical estimates [33]; an *ab initio* calculation for the Li + H_2 collision system is presently underway at NIST. Molecular hydrogen, H_2, is the most common and therefore important residual gas (mostly due to outgassing from stainless steel and other metals) in the ultra-high vacuum (UHV) pressure regime, and the Cold Atom Vacuum Standard (CAVS) will ultimately rely on precise knowledge of the theoretically determined Li + H_2 cross section. Other gases contribute as minor constituents of the background or as calibration or test gases purposefully introduced into the vacuum, such as N_2, H_2O, He, Ar, or CO_2. For these gases, the thermalized rates are expected to be on the order of 10^{-9} $\mathrm{cm^3\ s^{-1}}$ and vary by only about 20%. Consequently, in the UHV environment, where typically 95% of background gas is H_2, uncertainty in the exact composition of the remaining gas is a small contribution to the total uncertainty. For highest accuracy calibrations, ultra-high purity H_2 gas can be leaked into the CAVS. However, the CAVS can be used to directly measure the background gas. To be used as a background sensor, k_{loss} must be known for the constituent gases or, alternatively, a relative gas sensitivity factor (relative to k_{loss} for H_2) must be known. In practice, a gas sensitivity factor can be determined (theoretically or experimentally) relative to the known theoretically determined k_{loss} for H_2, thus transferring SI traceability to the gas sensitivity factors. Experimental determinations are discussed is section 5.6.

4. *Ab initio* calculations of atomic and molecular parameters

High accuracy, *ab initio* quantum calculations of the relationship of refractivity to pressure are only possible for helium gas at the present time, due to the complexity of other atoms or molecules. Only for helium can the refractivity be calculated much more accurately than it can be measured. The calculations thus provide a basis for determining pressure from refractivity measurements with an uncertainty below what is currently possible for pressure measurements. Recent results of Puchalski *et al* [20] are the most accurate to date and provide a strong theoretical foundation for helium refractivity. The central focus of this work was computing the atomic polarizability of helium with a fractional uncertainty of $1 \cdot 10^{-7}$ at optical frequencies. Relativistic and quantum eletrodynamics (QED) effects were included in the calculation. Finite-mass effects, including the leading relativistic correction, were also taken into account. Finite nuclear size effects were calculated and found to be essentially negligible. The uncertainty of the result was dominated by the uncertainty in the estimation of the α^4 QED correction to the static polarizability. It was argued that neglected terms, such as higher-order QED recoil corrections, should be negligible at the level of $1 \cdot 10^{-7}$. It was carefully ascertained that basis-set convergence errors also were negligible. There have been a number of previous calculations of the static polarizability of helium, most recently Łach *et al* [34], and there has been one previous *ab initio* calculation of the dynamic polarizability [35]. Differences between previous calculations and the result of Puchalski *et al* are well understood, indicating that the calculations are on a firm footing.

In addition to the polarizability calculation, Puchalski *et al* [20] reviewed previous work regarding diamagnetic susceptibility and virial coefficients for density and refractivity. The diamagnetic susceptibility has only been calculated for the static case but is sufficiently small that any likely frequency dispersion can be safely ignored. Combining these results with the new result for polarizability gives an *ab initio* theoretical result for refractivity as a function of temperature and pressure. Puchalski *et al* believe that the estimated fractional uncertainty is less than $1 \cdot 10^{-6}$ for pressures up to 3 MPa [20]. An experimental determination of the pressure independent static polarizability A_{R} with 2 ppm relative uncertainty [36] is in agreement with the theoretical work [20]. Throughout this document, 'uncertainty' always refers to standard uncertainty.

Concerning the electrical interactions, the second refractivity virial coefficient plays an important role. The difference between the second dielectric virial coefficient $b_{\mathrm{s}}(T)$, which is relevant for the static case, and the refractivity virial coefficient $b_{\mathrm{R}}(T)$ is small (at a wavelength of 632 nm at $T = 273.16$ K about 3% [37]). Therefore it is sufficient to refer to calculations of $b_{\mathrm{s}}(T)$, for which two fully quantum statistical *ab initio* calculations for helium are available [37, 38]. The difference between the values of these calculations is on the level of 10%. A recently performed calculation of $b_{\mathrm{s}}(T)$ in the semi-classical approximation [39] supports the value published in [37]. At the moment, the experimental data is not of sufficient uncertainty to judge between the two theories but for the pressure range shown in table 1, a 10% uncertainty is sufficient to perform accurate pressure measurements on the ppm level.

Similar to *a priori* quantum calculations of refractivity, *a priori* calculations for line intensities S are rather difficult and expensive due to the complexity of atoms or molecules. Accurate calculations of molecular line intensities require accurate dipole momentum and potential energy surfaces, both of which are generally not available. Nevertheless, Polyanski *et al* [40] succeeded to perform such calculations for $^{12}C^{16}O_2$ line intensities for the (20 012)–(00 001) band and obtained agreement with a recent experimental value [27] on the level of $6 \cdot 10^{-4}$ (relative difference between the experimental and theoretical values), within the uncertainty of the experimental value, however, amounting to $4.2 \cdot 10^{-3}$. At present, these values indicate the level of uncertainty that can be achieved by *ab initio* quantum calculations for line intensities S.

5. Experimental realizations of optical methods to determine number density

5.1. Refractive index measurement by fixed length optical cavity

A fixed-length optical cavity provides a relatively simple and straightforward mechanism for determining the refractive index of a gas. If a laser is servo-locked in resonance with a Fabry–Perot cavity filled with gas, the frequency f of the laser is given approximately by:

$$f = \frac{mc_0}{2nL}, \tag{33}$$

where m (the mode order) is the integer number of wavelengths in the cavity, and L is the length of the cavity. If gas density changes, causing n to change, the servo adjusts f so as to maintain resonance with the cavity. Hence frequency changes track changes in refractive index, in a manner governed by equation (33). If a measurement of the initial frequency f_i is made at vacuum, where $n = 1$ exactly, and a second measurement f_f is carried out at some pressure of interest, refractivity $(n - 1)$ can be determined from equation (33) applied to the two frequency measurements:

$$(n-1) = \frac{f_\mathrm{i} - f_\mathrm{f} + \Delta m \left(\frac{c_0}{2L}\right)}{f_\mathrm{f}}, \tag{34}$$

where Δm is the change in mode order between the initial and final measurements. A traditional method of determining the length L of the cavity or mode order m is to measure of the free spectral range (FSR) of the cavity [41, 42]; FSR measurements might be used to determine m and thus Δm, with proper consideration given to the effect of dispersion in the gas. Other approaches can also be used to determine Δm, where the simplest is to rely on approximate knowledge of the pressure, as measured by an ancillary gauge of modest accuracy, to derive an estimate for Δm that is rounded to the nearest integer.

When highest possible accuracy is required, it is also necessary to consider additional effects not captured in equation (33) or (34). In particular, determining the physical length L of the cavity via FSR measurements requires consideration of mirror phase shifts and, for sub- part-per-million accuracy, diffraction effects (the Gouy phase shift). More important, equation (34) must be modified to correct for an additional effect of significance, namely, the length of the cavity changes in response to pressure changes, as was mentioned in section 3.1. The resulting modifications to equation (34) due to Gouy phase, mirror phase shifts, and pressure-induced length changes are discussed in [7, 9]. See also the discussion of section 3.

The frequency f of the laser is determined by measuring the frequency difference between the laser and a reference laser of known frequency (beat frequency measurement). Lowest noise and drift and the least sensitivity to thermal variations can be achieved if the reference laser is servo locked to a second cavity, built on the same spacer as the measurement cavity, and held at vacuum at all times.

The NIST has designed a fixed-length optical cavity (FLOC) following the principles described above [9]. The cavity is shown in figure 1. Four mirrors are silicate bonded to the ends of a spacer. Two of the mirrors are bonded to the ends of the slot at the top of the device. This forms a Fabry–Perot cavity that is open to its surroundings and contains the gas for which the pressure is to be measured. In practice, the entire cavity is held in a copper chamber that forms a vacuum chamber. The other two mirrors are bonded to the ends of a hole to form an enclosed reference cavity that can be continuously pumped to vacuum. A pedestal (not visible in figure 1) is bonded to the bottom of the spacer body with a hole for pumping the reference cavity. The spacer body, mirror substrates, and pedestal are made from Corning ULE[4] (Ultra Low Expansion glass), silicate bonded together to form a near-monolithic structure. In equilibrium, the chamber is isothermal at the millikelvin level. The volume of the enclosure is minimized so as to minimize pV work that will disturb the thermal equilibrium when gas is admitted to the chamber.

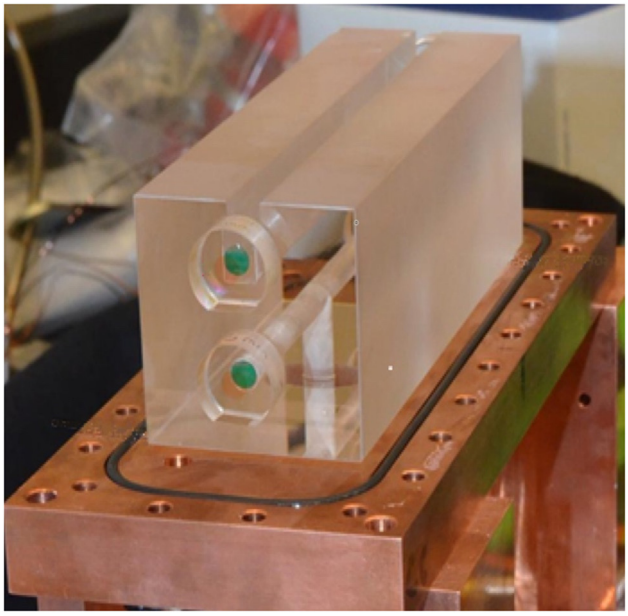

Figure 1. FLOC dual Fabry–Perot cavity, supported slightly above the copper base of a combined pressure chamber/thermal enclosure.

When the FLOC is used with a gas of known refractive index, the achievable uncertainty is limited by variations in the length of the cavities with changing pressure. The changes in length of the measurement cavity are almost entirely due to the bulk modulus of the material. The reference cavity has additional changes due to bending of the windows (the mirror substrates). These effects are easily corrected through a combination of measurements and calculations, but uncertainties in the bulk modulus and in the position of the resonant modes in the reference cavity limit the attainable accuracy [9, 22].

The FLOC potentially has a very broad range of operation from less than one pascal to 3 MPa. As mentioned in section 4, it is currently believed [20] that virial coefficients for helium are known with sufficient accuracy that the refractivity

[4] Certain commercial equipment is identified in this paper to adequately describe the experimental procedure. Such identification does not imply recommendation or endorsement by NIST or PTB, nor does it imply that the equipment identified is necessarily the best available for the purpose.

as a function of pressure can be calculated up to 3 MPa with less than 1×10^{-6} relative uncertainty which indicate that the FLOC could potentially replace part of the pressure scale that traditionally has been dominated by piston gauges. The variation of bulk modulus with pressure will cause a nonlinearity that must be taken into account; this has been measured for ULE [43]. The resulting nonlinearity in pressure measurement is about 10 μPa Pa^{-1} at 3 MPa. The uncertainty of this correction is currently estimated to be less than 1 μPa Pa^{-1}.

On the low pressure side, the FLOC has a potential operating range extending down to the regime of ionization gauges. The current NIST version is not optimized for low pressure operation but nevertheless shows good performance. When compared to an ionization gauge, the FLOC noise level was only 0.1 mPa for 1 s averages. In principle, sub micropascal measurements might be possible. Lasers locked to Fabry–Perot cavities near room temperature have achieved fractional frequency stabilities below 10^{-16} for averaging times on the order of 1 s [44, 45], where the basic limitation is thermal noise (in the mirror substrate, the coatings, and the cavity spacer). For typical gas species such as nitrogen, oxygen, and water vapour, this thermal noise floor corresponds to about 4×10^{-7} Pa. However, the stability degrades rapidly as the measurement time increases, and as a practical matter the measurement floor will be limited by thermal or temporal instabilities of the cavity and by outgassing.

5.2. Variable length optical cavity

The complications of pressure distortions in a fixed-length cavity (section 5.1) can be eliminated by working at constant pressure and using a cavity of variable length (VLOC) [46]. The basic concept is to measure the same physical displacement ΔL in vacuum and in gas. In the gas, the apparent displacement is $\Delta L' = n\Delta L$. From the measured vacuum displacement ΔL and the difference in the two measured displacements, $(n-1)\Delta L$, the refractivity $(n-1)$ can be determined. Then

$$n - 1 = \frac{\Delta L' - \Delta L}{\Delta L}. \tag{35}$$

One of the most important features of the system will be its ability to measure the refractive index of any gas put into the cavity with a measurement uncertainty that is lower than currently published values. Thus, the VLOC will provide the needed link between helium's refractive index determined from *ab initio* quantum calculations and the refractive index of a common calibration gas such as nitrogen. A variable-length system is nearing completion at NIST and will be used as a primary pressure standard with helium as the working medium.

One conceptual method of achieving this goal is shown in figure 2. This scheme employs four Fabry–Perot interferometers to measure optical lengths, based on frequency measurements of lasers locked to the cavities similar to what was previously described for the FLOC. Three are in vacuum and one in gas. The four interferometers are built on two baseplates. One baseplate is simply a flat plate of ULE glass that has four flat mirror coatings on the surface. The second baseplate has curved mirrors silicate bonded to a ULE plate. A bellows (not shown for clarity) allows for varying the length of the tube between the two baseplates, and one baseplate is mounted on a precision stage to change the cavity length. The tube encloses the centre interferometer and can be filled with gas while the outer interferometers are maintained at vacuum. The outer three interferometers measure the vacuum displacement and also monitor angular tilts of the moving baseplate.

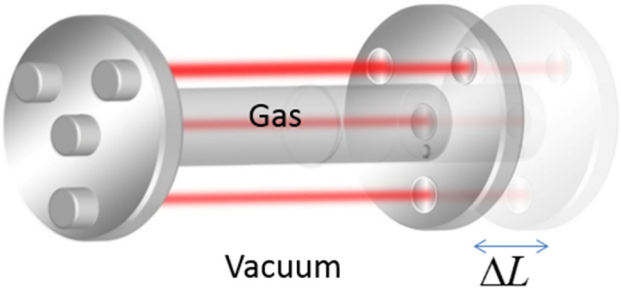

Figure 2. Conceptual drawing of variable length optical cavity.

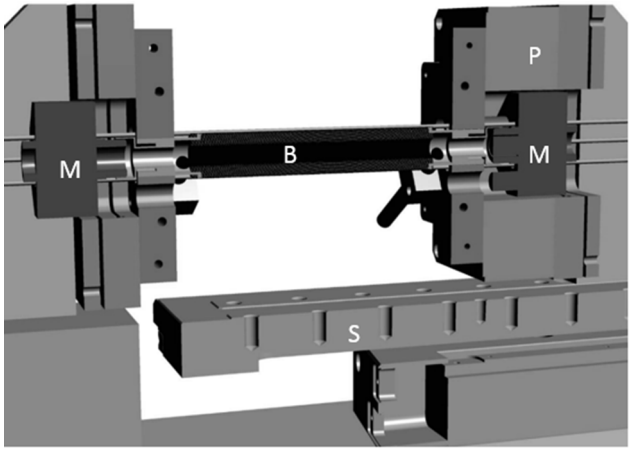

Figure 3. Cross-sectional view of the NIST VLOC, showing bellows section (B) ULE mirror assemblies (M). Piezo stage for tip-tilt control (P), and a portion of the translation stage (S).

The challenge of any such approach is to assure that the average change in physical length ΔL of the central Fabry–Perot cavity must be precisely the same as the change in average length of the outer three Fabry–Perot cavities. Our goal is to achieve a relative uncertainty of 1×10^{-6} in pressure measurements employing helium, which requires no more than 3 pm inequality in the displacements for a displacement of 15 cm. The near-monolithic baseplate structures establish the physical relationship between the internal and external interferometers with picometer stability, which is one requirement needed to assure that the displacements are equal. Possible pressure distortions are constant during a displacement measurement and therefore do not affect the measurement result, but bellows spring forces vary with displacement and might distort the relative positions of the mirrors on the baseplates. Finite element calculations show that, with careful design, the resulting errors can be kept below 1 pm.

The need for precise equality of the changes in physical lengths of the helium and vacuum cavities carries with it several demanding requirements. Perhaps the most demanding is

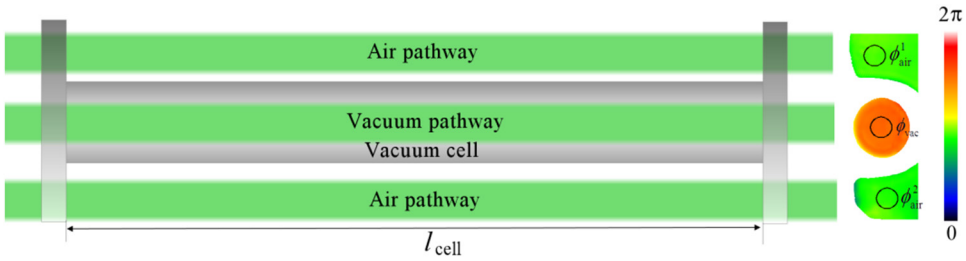

Figure 4. Scheme of pathways when using a vacuum cell for the interferometric measurement of the air refractive index. Reproduced from [48]

to minimize Abbe errors due to pitch and yaw of the moving optic. When angular motion errors are present, the average of the vacuum displacements will not equal the physical displacement of the central interferometer unless the location of the central cavity mode is carefully adjusted to zero Abbe offset. Even with the Abbe offset reduced to micrometers, it is still necessary to keep pitch and yaw errors at submicroradian levels. To eliminate pitch and yaw, we expect to use the three vacuum interferometers to measure pitch and yaw with sub-nanoradian precision and provide feedback to a piezo stage so as to maintain a constant orientation of the moving optic assembly relative to the fixed optic assembly.

Further considerations require that roll and straightness errors be minimized and that the cavity modes are aligned to each other and to the direction of stage motion at the microradian level [46].

A cross-sectional view of the final apparatus is shown in figure 3.

5.3. Interferometric method

The refractive index of air is an important parameter for interferometric length measurements of material measures, and for interferometric length measurements in air, the uncertainty in air refractive index can be one of the leading sources of error. For this reason, methods for the accurate determination of air refractive index have been established and refined. In case of using large field imaging interferometers, typically designed for the primary realization of the length of gauge blocks, it is preferable to determine the average air refractive index along the measured length interferometrically by using a vacuum cell as refractometer. In this approach a permanently evacuated vacuum cell is installed beside a gauge block to be measured and the air refractive index is determined from the comparison of optical path lengths in vacuum and air by interferometry. Figure 4 schematically shows such vacuum cell (left) with end faces that are closed by optical flat windows made of a homogenous transparent material. At the right side of figure 4, a typical interference phase topography, as from a measurement with PTB's Kösters-Interferometer [47], is shown. Circular regions of interest (ROIs) are defined at positions of the air pathway (top and bottom) and the vacuum pathway (centre) within which the (unwrapped) phase values are averaged.

The vacuum cell provides a common geometrical length, l_{cell}, valid for both, the pathway of light inside the vacuum cell and the pathway through air. l_{cell} can therefore be expressed in terms of multiples of interference orders (i: integer order, q: fractional order) in two different ways:

$$l_{\mathrm{cell}} = (i_{\mathrm{vac}} + q_{\mathrm{vac}})\,\frac{\lambda_{\mathrm{vac}}}{2} = (i_{\mathrm{air}} + q_{\mathrm{air}})\,\frac{\lambda_{\mathrm{vac}}}{2n}, \qquad (36)$$

in which the suffix 'vac' indicates the vacuum pathway and the suffix 'air' indicates the air path. According to equation (36) the refractivity of air can be written as:

$$n - 1 = \frac{(i_{\mathrm{air}} - i_{\mathrm{vac}} + q_{\mathrm{air}} - q_{\mathrm{vac}})\,\lambda_{\mathrm{vac}}/2}{l_{\mathrm{cell}}}. \qquad (37)$$

Using several light sources of different wavelengths λ_k, the corresponding integer interference orders, $\widetilde{i}_k = i_{\mathrm{air},k} - i_{\mathrm{vac},k}$, can be determined by utilizing a coincidence criterion [48]. The fractional order of interference, $\widetilde{q}_k = q_{\mathrm{air},k} - q_{\mathrm{vac},k}$, is obtained from the measured interference phase topography:

$$\widetilde{q}_k = \frac{1}{2\pi}\left[\frac{1}{2}\left(\phi^1_{\mathrm{air}} + \phi^2_{\mathrm{air}}\right) - \phi_{\mathrm{vac}}\right]_k, \qquad (38)$$

in which ϕ^1_{air}, ϕ^2_{air} and ϕ_{vac} denote averaged phase values obtained within the ROIs shown in figure 4, right. Installation of such interferometer equipment including a refractometer cell inside a vacuum chamber is possible, for example, with PTB's ultraprecision interferometer (UPI) [49], which allows extraction of zero offset length differences $\widetilde{q}_k \cdot \lambda_k/2$ when both the cell and the interferometer are evacuated. This offset is caused by refractive index inhomogeneities of the cell windows and is dependent on the window thickness and slightly on the wavelength, but also on the actual position of the cell windows with respect to the light beam (adjustment). The measured zero offset (up to 40 nm found for 10 mm thick windows) is used as a correction to equation (37). For highest accuracy measurements of air refractive index (e.g. as in [50]) such zero measurements are absolutely required.

In principle the above mentioned approach can be applied for any gas, not only air. According to the relationship $n_{\mathrm{gas}} - 1 = \frac{(i+q)\lambda_{\mathrm{vac}}/2}{l_{\mathrm{cell}}}$, the relative uncertainty $u(n_{\mathrm{gas}} - 1)/(n_{\mathrm{gas}} - 1)$ is equal to the quadrature sum of the relative uncertainties $u(\lambda_{\mathrm{vac}})/\lambda_{\mathrm{vac}}$ and $u(l_{\mathrm{cell}})/l_{\mathrm{cell}}$. Considering air under normal conditions as an example, relative uncertainty of 10^{-8} for λ_{vac} causes an absolute uncertainty contribution of only 2.8 10^{-12} for the air refractivity at 20 °C. Similarly, a typical relative uncertainty of 10^{-6} for l_{cell} causes an absolute uncertainty contribution of only 2.8 10^{-10}. The attainable uncertainty of $n_{\mathrm{gas}} - 1$, however, is limited by the uncertainty of the fractional interference order via

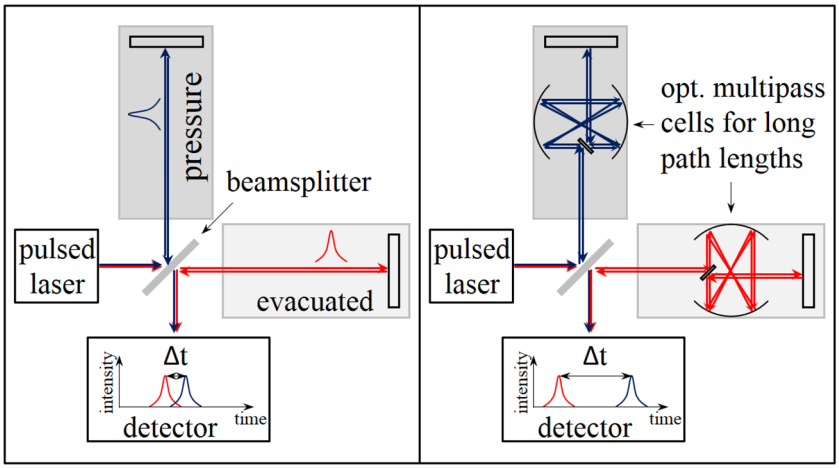

Figure 5. Michelson setup for optical time-of-flight measurements. (Left) With normal arms. (Right) Using optical multipass cells to increase the path lengths of both arms and thus the delay times and resolution.

the absolute contribution $\frac{\lambda_{\mathrm{vac}}/2}{l_{\mathrm{cell}}}u(q)$. In case of the UPI the fractional order of interference can be extracted on a level of about $3 \cdot 10^{-4}$ [49]. Consequently, a 420 mm long vacuum cell installed inside the UPI generally allows absolute gas refractivity measurements on a level approximately $3 \cdot 10^{-10}$. Considering additional uncertainties (including contributions for the offset correction and window deformation) an overall standard uncertainty of the air refractivity is estimated to be approximately $5 \cdot 10^{-10}$. This value is equivalent to a pressure variation of less than 0.2 Pa. Provided, that the air temperature measurement system/network is highly accurate, as it is for PTB's UPI, it is consequently possible to measure the 'normal' pressure of air by imaging interferometry on a relative level of approximately $2 \cdot 10^{-6}$.

5.4. Speed of light measurement

Equation (10) can be used to measure the refractive index by the speed of light in a gas medium. Different experimental set-ups are possible. A light pulse can be sent along a known path length and the time measured for this length. Also, a continuous EM-wave may be modulated with a relatively low frequency (compared to the optical frequency) in the MHz range and be sent to a detector via two different paths of known length. The phase difference between the two paths is measured.

Measurement range and resolution are improved with the use of shorter pulses and longer path lengths. Figure 5 shows a set-up, where the time difference is measured between two identical geometrical paths. One path travels through an evacuated chamber, the second through a chamber with a gas medium. By using multi-pass cells the time difference between the two branches can be increased (right part in figure 5).

When femtoseconds lasers are used, refractive index n for a single wave length has to be replaced by the group refractive index $\widetilde{n}$. The time difference Δt of the beams through two branches, one in vacuum with c_0, one in a gas medium with $c_0/\widetilde{n}$, but identical length l, is given by

$$\Delta t = (\widetilde{n} - 1)\,\frac{l}{c_0}. \tag{39}$$

With a laser pulse of about 30 fs duration a time resolution of about $\delta t = 3$ fs should be possible by a cross-correlation measurement [51]. With $l = 30$ km this gives a resolution of the refractivity $\delta\,(\widetilde{n} - 1)$ of $3 \cdot 10^{-11}$, which, for helium with a refractivity of $3 \cdot 10^{-5}$ (100 kPa, 296 K), gives a relative uncertainty due to resolution of 10^{-6}.

If a frequency resolved technique is used for the cross-correlation measurement, the additional benefit of a frequency spectrum allows to compare the measured dispersion with the *ab initio* calculated dynamic polarizability which is more uncertain than the static polarizability. Such a technique is the frequency-resolved optical gating (FROG) [52].

In addition to resolution, there are uncertainty contributions from temperature, from thermal expansion, pulse dispersion, and compression caused by the increase of pressure of the gas, which all should be of the same order of 10^{-6} (relative).

Compression of the mirror materials leads to a change of radius of curvature in a multipass cell. With the use of a special type [53] of multireflection cell after Herriott [54], however, a change in the ratio of radius of curvature divided by the mirror distance leads to a beam walk of the out-coupled beam. By controlling the mirror distance with respect to an external reference and consideration of the beam walk, the influence of compression can be corrected.

Pulse dispersion may be solved in the future by measuring the pulse delay not in the time domain, but frequency domain with a dual frequency comb [55]. This may also greatly improve the resolution in optical path length, but present state of the art has not advanced far enough for this review to give more details.

To limit the contribution of the temperature to a relative uncertainty of 10^{-6} in pressure, 0.3 mK uncertainty is needed. With vacuum vessels of dimensions to host beam path lengths in the kilometer range, this is not realistic. If, however uncertainties of a factor of 10 higher can be accepted, the speed of light measurement is a useful, but expensive, method to

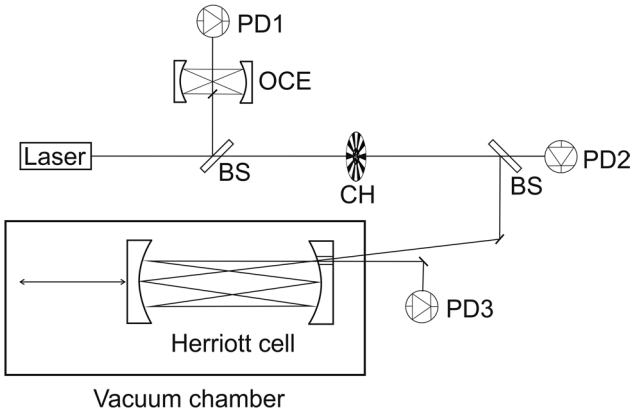

Figure 6. Experimental set-up of a gas density measurement by the absorption method [57]. BS beam splitter, OCE open confocal etalon, CH chopper, PD photo detector, no. 1 for frequency determination, 2 for laser intensity (reference), 3 for absorption signal. The chopper is used for lock-in-detection of the signals from PD2 and 3. The position of the left mirror of the Herriott cell in the vacuum chamber can be changed *in situ*.

measure gas pressure. The effort includes a fs-laser, a fast and sensitive detector, mirrors with large diameters and corresponding large vacuum chambers with a temperature stability of several millikelvin. One must keep in mind, that the spectrum of the laser emission should be far away from any possible absorption lines of the used gas. In addition, the laser power must be small enough, so that the laser beam itself is not changing the refractivity, for example by non-linear effects or by building up a plasma [56].

5.5. Absorption method

The absorption experiment needs a laser as a monochromatic source of an EM wave with frequency ν, a detector suitable for the frequency ν, and a well defined path length of the EM wave through the absorbing medium.

For a fundamental method, it is necessary to determine the full integral of the absorbing line as described in equation (27). To this end, the laser has to be tuned not only across the absorption line, but also far outside from it to detect I_0. The Lorentz-part of the form function compared to the Gaussian part decreases quite slowly with distance from the line centre: About 100 times of the full width at half maximum (FWHM) are needed to reduce intensity to a level of 10^{-4} of the peak height. Since pressure broadening increases the FWHM of the Lorentz-part, it is rather difficult to accurately determine the integral at higher pressures (>100 Pa). Fortunately, the FWHM of the Gaussian part is much larger than that of the Lorentz part, even in the infrared.

The molecular transition must be carefully selected so that it can be assumed that no other transition nearby the absorption line disturbs the measurement of I_0.

To achieve a reasonable resolution, the absorption paths need to be enlarged, e.g. by multi-pass cells. Herriott cells [54] are very useful for this purpose, because the path length can be easily changed and determined with an uncertainty $<10^{-3}$. In a Herriott cell, at particular distances of the mirrors the number of reflections within the cell is defined and therefore so is the path length.

Figure 6 shows an experimental set-up for a gas density measurement by absorption method [57]. The beam is split into three channels. One channel is used to calibrate the frequency or wave number axis *in situ*, the second channel to normalize the detector to intensity changes of the laser, the third is the measuring channel. A special feature of the experimental set-up shown in figure 6 is that the absorption length can be changed by about one order of magnitude (from 6 m to 70 m) by a movable mirror, with still enough intensity for measurement.

With such a set-up and full traceability of all auxiliary equipment it is possible to achieve an uncertainty of pressure realization for CO_2 of 0.5 % in the range from about 10 Pa to 1 kPa with the largest contribution from uncertainty of line intensity [27].

Another powerful method to increase the effective optical path length is cavity-ring-down-spectroscopy (CRDS) [58]. For this technique, a laser beam is injected into a high finesse cavity consisting of two mirrors (figure 7). When the laser frequency is in resonance with the cavity, intensity in the cavity builds up to a maximum determined by the quality of the resonator (cavity finesse), a factor on the order of 10^5. If the incoming beam is suppressed suddenly, an exponentially decaying intensity leaks out of the cavity. This decay rate depends on losses caused by the imperfect reflectivity of the mirrors, scattering (Rayleigh, Mie), and (of primary interest here) molecular absorption. The effective beam path in the cell may amount to several kilometers for a cavity a few centimeters long. The comparison of the decay times for the evacuated cavity and for the same cavity filled with the gas of interest allows for the calculation of the molecular absorption. The calculation is based on a modified version of equation (22):

$$I(\nu, t) = I_0(\nu) \exp\{-t/\tau(\nu)\} \tag{40}$$

where the decay time $\tau(\nu)$ is given by

$$\tau(\nu) = \frac{n}{c} \cdot \frac{l}{1 - R - X - l \cdot k(\nu)}. \tag{41}$$

Here l is the distance between the mirrors, R is the reflectivity and X are the losses caused by scattering. For high finesse cavities, effective dwell times per photon inside the cavity of 100 µs are easily achieved even within small dimensions of some decimetres, corresponding to an effective optical path length of 30 km.

With the combination of sufficient laser power and a finesse that is high enough, it is possible to saturate the molecular absorption, leading to a transparent medium. In that case, it is possible to measure in one step without evacuating the cavity, simply by comparing the first part of the decay curve, with the second part. The first part is accompanied by a decay time equal to that of an evacuated cavity, caused by the saturation effect, while the second part is affected additionally by the molecular absorption. This technique is called saturated-absorption CRDS (SCAR) [59]. With SCAR it was already possible to achieve a resolution of 43 parts in 10^{15} (ppq) in

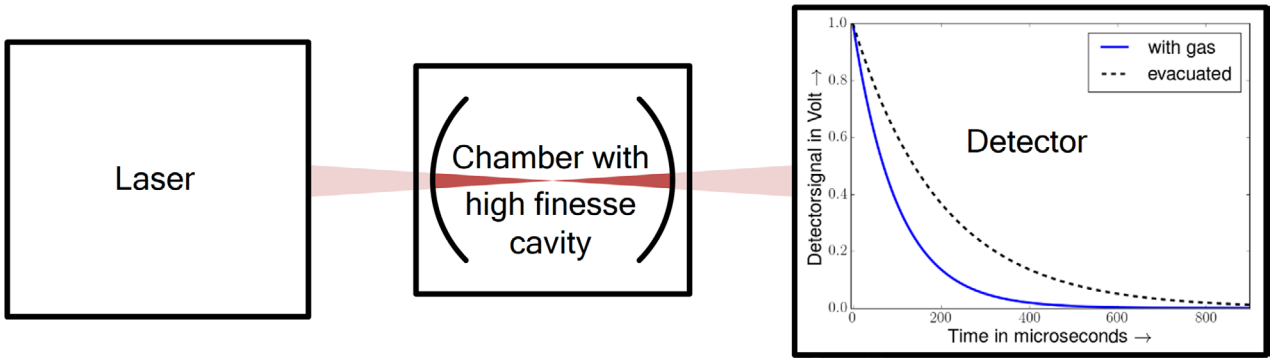

Figure 7. Principle of cavity-ring-down-spectroscopy. The laser's power output can be switched off within several nanoseconds, e.g. by the use of a pockels cell. The cavity mirrors have a high finesse in the order of several thousand. The detector must be fast enough to resolve the delay times. Typically, a cooled detector is used, to enhance the signal to noise ratio.

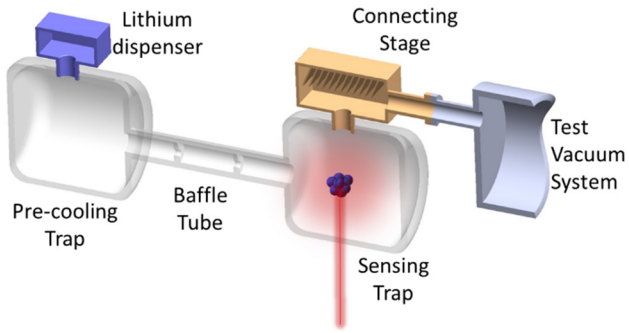

Figure 8. Schematic representation of the proposed cold-atom vacuum standard (CAVS).

$^{14}CO_2$ detection [60]. This corresponds to a partial pressure of $4.3 \cdot 10^{-9}$ Pa and is therefore not far from the XHV.

5.6. Cold atom traps

Cold atom traps have the potential to measure the lowest gas densities by optical methods, i.e. in ultrahigh vacuum (UHV) and extreme high vacuum (XHV). NIST and others are presently exploring using ultra-cold atoms to sense the absolute number density of molecules in vacuum [61–65], the NIST project is explained in more detail in an accompanying article also in this issue [66].

Figure 8 represents a potential prototype cold-atom vacuum standard (CAVS) using Li as a sensor atom that is currently under construction at NIST. Initial laser-cooling and trapping of atoms is done in the pre-cooling trap region, creating a needle-like beam of atoms that flow through the baffle tube into the sensing trap. These atoms are now are further cooled to sub-millikelvin temperatures and held in a magnetic trap, at which point they become sensor atoms. A gas molecule in the vacuum may strike a sensor atom, knocking it out of the trap, so the loss rate of atoms from the trap becomes a measure of background particle number density. The number of atoms in the trap is detected using photonic techniques, such as absorption imaging. The pressure of the test vacuum system is determined from the loss rate of Li atoms from the sensing trap according to equation (30).

To develop the CAVS, the loss-rate coefficients must be both theoretically and experimentally determined. NIST will experimentally determine cross sections or rate-coefficients for collisions of cold alkali-metal atoms with H_2 and many other molecules by building a dynamic expansion standard in tandem with the CAVS, which allows us to generate a known gas pressure in the CAVS. By setting a known pressure and measuring the trap lifetime, the cross sections leading to trap loss are determined. In parallel, NIST will develop accurate theoretical and efficient computational models to determine the collision rate coefficient between the Li alkali metal atoms and the background gas. Comparison between these and the experimentally determined loss rates will be essential for validating our methods and uncertainty. Ultimately, a primary CAVS will depend upon theoretically calculated loss-rate coefficients and relative gas sensitivity factors (relative to H_2) as discussed in detail in the companion paper appearing in this issue [66].

Other challenges to creating the absolute CAVS include understanding and, where possible, preventing other mechanisms that lead to atom loss from the trap. For example, atom-loss due to non-adiabatic spin-flip transitions as the trapped atoms move toward a region of zero magnetic field can be avoided by careful design of the magnetic trap. Similarly, the effect of background atoms colliding with trapped cold atoms with a glancing angle, which lead to heating but not loss, can be minimized by making the magnetic trap shallow. Collisions between two or more cold atoms in the trap can also lead to trap loss, but these are avoided by maintaining a low density of trapped cold atoms. In our case, the mean free path of the cold atoms will be on the order of 10 m but the cold atom cloud is on the order of micrometer.

This new way to realize UHV and extreme-high vacuum is both a primary standard and a sensor of vacuum. Ultimately, it is photon-based metrology because the number of sensor atoms in the trap is photonically-probed.

6. Discussion

Gas density compared to pressure is the more appropriate quantity to characterize the vacuum state. Optical methods have an advantage in that they are based on the number density of gas in the vacuum and these are accessible through interactions of light with matter. It has been shown by NIST [10] that optical methods can become fundamental standards

and have the potential to provide a new route of SI traceability for the pascal.

The refractive index method with an optical cavity of variable length has the pospect of becoming the most accurate method to realize pressure and gas density. The NIST VLOC is projected to achieve an uncertainty near 1 part in 10^6, significantly better than what has been achieved by manometers and comparable to what has been recently achieved with piston gauges [67].

The FLOC is a simpler, more robust device than is the VLOC, suitable for wider use beyond NMIs. Its primary disadvantage relative to the VLOC is that it is subject to pressure-induced changes in the mechanical length of the cavities, which must be measured and corrected or calculated from known values of material elastic constants. For pressures above 100 Pa, best performance will probably be achieved if the pressure distortions are evaluated by comparison of FLOC pressure measurements to the VLOC.

An attractive alternative is to employ the FLOC as an independent standard using two gasses for which the relationship of refractivity to pressure is well known, either from theory (for helium) or from experimental measurements (potentially measured to high accuracy with the VLOC). This can be done without requiring direct comparison to a known pressure standard, working under the assumption that the only significant error in the FLOC is pressure distortion. If, for example, measurements of refractivity are made for helium and nitrogen with both at the same pressure (where the pressure need not be known), then the two measured refractivities can be used to determine two unknowns; (a) the unknown pressure and (b) the pressure distortion of the FLOC. In effect, the known refractivities of the two gasses serve as a mechanism for traceable dissemination of the Pascal where traceability is provided by the atomic/molecular properties of the gasses in place of a direct comparison to a primary standard. (Except in the case of helium, there is indirect comparison to the pressure standard that was used when the gas refractive index was determined experimentally.) The uncertainty of pressure measurement using the two-gas dissemination method is potentially a few parts in 10^6 at atmospheric pressure, if the refractivity of nitrogen can be measured with comparable uncertainty. Note that it is still necessary to separately establish traceability of the FLOC temperature sensor and the time base for frequency measurements.

If the FLOC is tested with three known gasses, this will uncover any possible contamination of one of the gasses used for pressure dissemination. Three-gas tests combined with other internal consistency checks can be used to verify continued proper operation of all components of the system other than the temperature sensor. This subject is treated in detail in a coming publication [22].

With this distortion correction, the FLOC should be able to extend the high accuracy of the VLOC to a much broader pressure range, conceivably spanning 9 orders of magnitude from millipascal to megapascal.

For argon no *ab initio* calculations of polarizability on the ppm level are available. This, however, may change in the future by combining accurate DCGT (dielectric-constant gas thermometry [21]) measurements of the static polarizability with *ab initio* calculations of the frequency dependence and the magnetizability. New *ab initio* calculations of the virial coefficients have been performed during the last years [18, 68–71]. After experimental proof of these data, argon can be used as measuring gas. With the eight times larger polarizability, argon holds the advantage of being less sensitive to impurities and deformation under pressure.

The absorption method has been proved to be suited as a primary standard [4] in the high and medium vacuum, with the uncertainty of pressure realization below 1 %. For high sensitivity, long path lengths are needed which increases the effort.

The refractivity, speed-of-light and absorption measurements may benefit from using two or more detection frequencies. Redundancy is increased, but also important parameters may be analyzed at the same time. e.g. with cavities, the influences of compression may be distinguished from refractivity, for absorption, there is an additional measurement of temperature, and in the VLOC, measurements of dispersion would uncover any possible contamination of the helium in the cavity. From the technical point of view, however, the use of different frequencies increases complexity and a number of technical details have to be considered. Future investigations should reveal where the effort of using multiple frequencies will be beneficial.

One might point out that all optical methods are gas species sensitive. Comparing this to the present methods of pressure realization in the vacuum regime, however, one can note that all these methods require knowledge of the gas composition. In the case of a static expansion system [72], corrections for real gas behavior is needed, and in continuous expansion systems the dependence of conductances on gas species is needed [72]. In addition, also with the present methods, not all gas species are suitable for pressure realization, e.g. condensation or adsorption must be avoided. In addition, we should note that many types of vacuum gauges are gas sensitive and require a pure gas for calibration.

For the CAVS, the collision cross sections and therefore the loss-rate coefficients are expected to have minimal dependence on gas species composition in the vacuum in most cases, and thus the CAVS represents a large improvement over existing sensor technology in the UHV and XHV regions. Moreover, when considered as a standard, it is fundamental and based on *ab initio* quantum mechanical theory. In contrast, the current state of the art standard at the lowest pressures, the continuous expansion method [72], produces a known, calculated pressure in a chamber and is intrinsically not primary because it scales down the pressure from a calibrated gauge. Continuous expansion systems are standards to calibrate gauges, not themselves sensors. The CAVS is both a standard and a sensor, and it is this duality that will ultimately make the CAVS a disruptive technology, because it is intrinsically fundamental and delivers a zero-length traceability chain. Its practicality and applicability will be further advanced through efforts to miniaturize the atom trap and its supporting photonics and optics.

7. Conclusions

For over three and half centuries, we have relied upon the mercury manometer and for the past century on piston gauges for traceability to the pascal. This realization method was based upon measurements of force per area. While this has served the community well for high pressure, optical methods are now emerging to replace these measurement methods in the vacuum regime and perhaps up to 3 MPa. The optical methods intrinsically measure gas number density. In the vacuum regime, it may be advantageous to shift emphasis away from pressure toward number density, which is much more relevant for low pressure applications and which eliminates the uncertainty associated with temperature measurement. At higher pressures, force per area will continue to be relevant, but in this regime also the optical density measurements have significant strengths and can improve pressure measurement capabilities.

The paper has presented optical measurements methods of gas density that are promising from today's viewpoint. It remains to be seen which methods will dominate and which methods may face technological challenges limiting widespread adoption.

Acknowledgments

The authors thank NIST cold-collision theorists Eite Tiesinga and Constantinos Makrides for their enlightening discussions.

References

[1] Milton M J T, Richard Davis R and Fletcher N 2014 Towards a new SI: a review of progress made since 2011 *Metrologia* **51** R21–30
[2] White D R and Fischer J 2015 The Boltzmann constant and the new kelvin *Metrologia* **52** S213–6
[3] Fischer J 2015 Progress towards a new definition of the kelvin *Metrologia* **52** S364
[4] Jousten K, Padilla G and Bock T 2008 Investigation on tunable diode laser absorption spectroscopy for its application as primary standard for partial pressure measurements *J. Phys.: Conf. Ser.* **100** 092005
[5] Pendrill L R 2004 Refractometry and gas density *Metrologia* **41** S40–51
[6] Hedlund E and Pendrill L R 2006 Improved determination of the gas flow rate for UHV and leak metrology with laser refractometry *Meas. Sci. Technol.* **17** 2767–72
[7] Egan P and Stone J A 2011 Absolute refractometry of dry gas to ±3 parts in 10^9 *Appl. Opt.* **50** 3076–86
[8] Silander I *et al* 2013 Optical measurement of the gas number density in a Fabry–Perot cavity *Meas. Sci. Technol.* **24** 105207
[9] Egan P F *et al* 2015 Performance of a dual Fabry–Perot cavity refractometer *Opt. Lett.* **40** 3945–8
[10] Egan P F, Stone J A, Ricker J E and Hendricks J H 2016 Comparison measurements of low pressure between a laser refractometer and ultrasonic manometer *Rev. Sci. Instrum.* **87** 053113
[11] 2006 *The International System of Units (SI)* 8th edn (Sèvres: BIPM)
[12] Szwemin P 2008 How to characterize gas in high vacuum? *Vacuum* **82** 174–7
[13] Fellmuth B *et al* 2016 The kelvin redefinition and its mise en pratique *Phil. Trans.* R **374** 20150037
[14] Hurly J J and Moldover M R 2000 *Ab initio* values of the thermophysical properties of helium as standards *J. Res. Natl Inst. Stand. Technol.* **105** 667
[15] Cencek W *et al* 2012 Effects of adiabatic, relativistic, and quantum electrodynamics interactions on the pair potential and thermophysical properties of helium *J. Chem. Phys.* **136** 224303
[16] Bich E, Hellmann R and Vogel E 2007 *Ab initio* potential energy curve for the helium atom pair and thermophysical properties of the dilute helium gas. II. Thermophysical standard values for low-density helium *Mol. Phys.* **105** 3035
[17] Gaiser C, Fellmuth B and Zandt T 2014 Dielectric-constant gas thermometry and the relation to the virial coefficients *Int. J. Thermophys.* **35** 395–404
[18] Garberoglio G, Moldover M R and Harvey A H 2011 Improved first-principles calculation of the third virial coefficient of helium *J. Res. Natl Inst. Stand. Technol.* **116** 729
[19] Born M and Wolf E 1980 *Principles of Optics* (Oxford: Pergamon) ch 2
[20] Puchalski M, Piszczatowski K, Komasa J, Jeziorski B and Szalewicz K 2016 Theoretical determination of polarizability dispersion and refractive index of helium *Phys. Rev.* A **93** 032515
[21] Gaiser C, Zandt T and Fellmuth B 2015 Dielectric-constant gas thermometry *Metrologia* **50** S217–26
[22] Stone J A, Egan P F, Ricker J E and Hendricks J H Dissemination of SI pressure via measuring the refractive index of gasses, submitted
[23] Demtröder W 2003 *Laser Spectroscopy* 3rd edn (Berlin: Springer) ch 3
[24] Hartmann J-M, Boulet C and Robert D 2008 *Collisional Effects on Molecular Spectra: Laboratory Experiments and Model, Consequences for Applications* (Amsterdam: Elsevier) pp 79–83
[25] Weideman J A C and Siam J 1994 *Numer. Anal.* **31** 1497
[26] Ouyang X and Varghese P L 1989 *Appl. Opt.* **28** 1538
[27] Casa G C *et al* 2008 Primary gas thermometry by means of laser-absorption spectroscopy: determination of the Boltzmann constant *Phys. Rev. Lett.* **100** 200801
[28] Truong G-W, Anstie J D, May E F, Stace T M and Luiten A N 2015 Accurate lineshape spectroscopy and the Boltzmann constant *Nat. Commun.* **6** 8345
[29] Wübbeler G, Padilla Víquez G J, Jousten K, Werhahn O and Elster C 2011 Comparison and assessment of procedures for calculating the $R(12)$ line strength of the $\nu_1 + 2\nu_2 + \nu_3$ band of CO_2 *J. Chem. Phys.* **135** 204304
[30] Bjorkholrn J E 1988 Collision-limited lifetimes of atom traps *Phys. Rev.* A **38** 1599
[31] Gott Y V, Ioffe M S and Tel'kovskii V G 1962 *Nucl. Fusion* **3** 1045
[32] Pritchard D E 1983 Cooling neutral atoms in a magnetic trap for precision spectroscopy *Phys. Rev. Lett.* **51** 1336
[33] Bali S, O'Hara K M, Gehm M E, Granade S R and Thomas J E 1999 Quantum-diffractive background gas collisions in atom-trap heating and loss *Phys. Rev.* A **60** R29
[34] Łach G, Jeziorski B and Szalewicz K 2004 Radiative corrections to the polarizability of helium *Phys. Rev. Lett.* **92** 233001
[35] Bhatia A K and Drachman R J 1998 Optical properties of helium including relativistic corrections *Phys. Rev.* A **58** 4470

[36] Gaiser C *et al* 2017 Final determination of the Boltzmann constant by dielectric-constant gas thermometry *Metrologia* **54** 280
[37] Rizzo K A, Hättig C, Fernández B and Koch H 2002 The effect of intermolecular interactions on the electric properties of helium and argon. III. Quantum statistical calculations of the dielectric second virial coefficients *J. Chem. Phys.* **117** 2609
[38] Moszynski R, Heijmen T G A and Avorid A 1995 Second dielectric virial coefficient of helium gas: quantum-statistical calculations from an *ab initio* interaction-induced polarizability *Chem. Phys. Lett.* **247** 440
[39] Cencek W, Komasa J and Szalewicz K 2011 Collision-induced dipole polarizability of helium dimer from explicitly correlated calculations *J. Chem. Phys.* **135** 014301
[40] Polyansky O L, Bielska K, Ghysels M, Lodi L, Zobov N F, Hodges J T and Tennyson J 2015 High accuracy CO_2 line intensities determined from theory and experiment *Phys. Rev. Lett.* **114** 243001
[41] Bay Z 1971 The use of microwave modulation of lasers for length measurements *Natl Bur. Stand.* **343** 59–62
[42] Lawall J R 2005 *J. Opt. Soc. Am.* A **22** 2786
[43] Gerlich D, Wolf M, Yaacov I and Nissenson B 1976 Thermoelastic properties of ULE® titanium silicate glass *J. Non-Cryst. Solids* **21** 243–9
[44] Häfner S, Falke S, Grebing C, Vogt S, Legero T, Merimaa M, Lisdat C and Sterr U 2015 8×10^{-17} fractional laser frequency instability with a long room-temperature cavity *Opt. Lett.* **40** 2112–5
[45] Jiang Y Y, Ludlow A D, Lemke N D, Fox R W, Sherman J A, Ma L-S and Oates C W 2011 Making optical atomic clocks more stable with 10^{-16} level laser stabilization *Nat. Photon.* **5** 158–61
[46] Stone J A, Egan P F, Gerty D, Hendricks J H, Olson D A, Ricker J E, Scace G E and Strouse G F 2013 Picometer metrology for precise measurement of refractive index, pressure, and temperature *NCSL Int. Meas.* **8** 67–73
[47] Decker J E, Schödel R and Bönsch G 2003 Next generation Kösters interferometer *Proc. SPIE* **5190** 14–23
[48] Schödel R 2015 Utilisation of coincidence criteria in absolute length measurements by optical interferometry in vacuum and in air *Meas. Sci. Technol.* **26** 084007
[49] Schödel R *et al* 2012 A new ultra precision interferometer for absolute length measurements down to cryogenic temperatures *Meas. Sci. Technol.* **23** 094004
[50] Bönsch G and Potulski E 1998 Measurement of the refractive index of air and comparison with modified Edlen's formulae *Metrologia* **35** 133–9
[51] Iaconis C and Walmsley I A 1998 Spectral phase interferometry for direct electric-field reconstruction of ultrashort optical pulses *Opt. Lett.* **23** 792–4
[52] Kane D J and Trebino R 1993 Characterization of arbitrary femtosecond pulses using frequency-resolved optical gating *IEEE J. Quantum Electron.* **29** 571–9
[53] Padilla G 2013 *US Patent* 2013/0050704 A1
[54] Herriott D R, Kogelnik H and Kompfner R 1964 *Appl. Opt.* **3** 523
[55] Wu G, Takahashi M, Arai K, Inaba H and Minoshima K 2013 Extremely high-accuracy correction of air refractive index using two-colour optical frequency combs *Sci. Rep.* **3** 1894
Wu G, Takahashi M, Arai K, Inaba H and Minoshima K 2014 Extremely high-accuracy correction of air refractive index using two-colour optical frequency combs *Sci. Rep.* **4** 5789 (corrigendum)
[56] Braun A, Korn G, Liu X, Squier D J and Mourou G 1995 Self-channeling of high-peak-power femtosecond laser pulses in air *Opt. Lett.* **20** 73–5
[57] Padilla-Víquez G, Koelliker-Delgado J, Werhahn O, Jousten K and Schiel D 2007 Traceable CO_2-R(12) line intensity for laser-spectroscopy-based gas analysis near 2 μm *IEEE Trans. Instrum. Meas.* **56** 529–33
[58] O'Keefe A and Deacon D A G 1988 Cavity ring-down optical spectrometer for absorption measurements using pulsed laser sources *Rev. Sci. Instrum.* **59** 2544–51
[59] Giusfredi G *et al* 2010 Saturated-absorption cavity ring-down spectroscopy *Phys. Rev. Lett.* **104** 110801
[60] Galli I *et al* 2011 Molecular gas sensing below parts per trillion: radiocarbon-dioxide optical detection *Phys. Rev. Lett.* **107** 270802
[61] Fagnan D E, Wang J, Zhu C, Djuricanin P, Klappauf B G, Booth J L and Madison K W 2009 Observation of quantum diffractive collisions using shallow atomic traps *Phys. Rev.* A **80** 022712
[62] Arpornthip T and Sackett C A 2012 Vacuum-pressure measurement using a magneto-optical trap *Phys. Rev.* A **85** 033420
[63] Yuan J, Ji Z, Zhao Y, Chang X, Xiao L and Jia S 2013 A simple, reliable, and no-destructive method for the measurement of vacuum pressure *Appl. Opt.* **52** 6195–200
[64] Makhalov V B, Martiyanov K A and Turlapov A V 2016 Primary vacuometer based on an ultracold gas in a shallow optical dipole trap *Metrologia* **53** 1287–94
[65] Ahmed Z, Klimov N N, Douglass K, Fedchak J, Scherschligt J, Hendricks J, Ricker J and Strouse G 2016 Photonics enabled quantum metrology of temperature, pressure, and vacuum *Dekker Encyclopedia of Nanoscience and Nanotechnology* 3rd edn (London: Taylor and Francis)
[66] Scherschligt J, Fedchak J A, Barker D, Eckel S, Klimov N, Makrides C and Tiesinga E Development of a new UHV/XHV pressure standard (cold atom vacuum standard) *Metrologia* **52**
[67] Zandt T, Sabuga W, Gaiser C and Fellmuth B 2015 Measurement of pressures up to 7 MPa applying pressure balances for dielectric-constant gas thermometry *Metrologia* **52** S305–13
[68] Jäger B, Hellmann R, Bich E and Vogel E 2011 *Ab initio* virial equation of state for argon using a new nonadditive three-body potential *J. Chem. Phys.* **135** 084308
[69] Moldover M R *et al* 2014 Acoustic gas thermometry *Metrologia* **51** R1–19
[70] Cencek W *et al* 2013 Three-body nonadditive potential for argon with estimated uncertainties and third virial coefficient *J. Phys. Chem.* A **117** 7542
[71] Vogel E, Jäger B, Hellmann R and Bich E 2010 *Ab initio* pair potential energy curve for the argon atom pair and thermophysical properties for the dilute argon gas. II. Thermophysical properties for low-density argon *Mol. Phys.* **108** 3335
[72] Jousten K (ed) 2016 *Handbook of Vacuum Technology* 2nd edn (New York: Wiley) ch 15